Article

Not peer-reviewed version

Comprehensive Profiling of Banana Ripening (*Musa* spp.) Through Multivariate Analysis of Biochemical Attributes

Fabricio Guevara-Viejó , Delia Dolores Noriega Verdugo , Roberto Ivan Basurto Quilligana , Juan Diego Valenzuela-Cobos * , Miguel Javier Yuqui Ketil

Posted Date: 28 February 2026

doi: 10.20944/preprints202602.2040.v1

Keywords: banana; *Musa* spp.; ripening; postharvest; fruit quality; multivariate analysis; PCA; PERMANOVA; functional stages

 doi:10.20944/preprints202602.2040.v1

Article

Comprehensive Profiling of Banana Ripening (*Musa* spp.) Through Multivariate Analysis of Biochemical Attributes

Fabricio Guevara-Viejó, Delia Dolores Noriega Verdugo, Roberto Ivan Basurto Quilligana, Juan Diego Valenzuela-Cobos * and Miguel Javier Yuqui Ketil

Universidad Estatal de Milagro, Milagro, Provincia del Guayas, Ecuador,091050

* Correspondence: jvalenzuelac@unemi.edu.ec

Abstract

Banana ripening is a complex biological process that determines fruit quality and shelf life, yet the integrated behavior of physicochemical, nutritional, and enzymatic attributes throughout ripening remains insufficiently understood. This study applied a multivariate approach to characterize and classify Ecuadorian bananas across nine ripening stages (T1–T9). Twenty-seven samples (three replicates per stage) were analyzed considering 29 variables, including carbohydrates, proximate composition, minerals, vitamins, color, texture, and enzymatic activity (PPO and POD). Data were evaluated using PERMANOVA, Principal Component Analysis (PCA), Spearman's correlation, and k-means clustering. PERMANOVA confirmed that ripening stage explains nearly all multivariate variation (pseudo-F = 2758.3; R^2= 0.999; p = 0.001). PCA revealed a dominant gradient (Dim1 = 86.2%) describing a coordinated transition from green stages characterized by high starch content, firmness, and mineral concentration to overripe stages associated with sugar accumulation, increased PPO/POD activity, and tissue softening. Vitamin C reached its maximum value at the intermediate stage (T5). These findings indicate that banana ripening follows a synchronized physiological gradient, allowing the identification of functional ripening stages based on multivariate signatures, which may support improved postharvest management and the development of non-destructive monitoring strategies aligned with sustainable food systems.

Keywords: banana; *Musa* spp.; ripening; postharvest; fruit quality; multivariate analysis; PCA; PERMANOVA; functional stages

1. Introduction

Bananas (Musa spp.) are among the most important fruit crops in tropical agro-export systems and play a significant role in developing economies [1,2]. They are also strategic for food security due to their wide availability, affordability and nutritional contribution (FAO, 2020). From a compositional standpoint, bananas provide readily available carbohydrates, dietary fibre, and essential micronutrients, reinforcing their importance in various socioeconomic contexts [4–6]. In Ecuador, their economic importance is closely linked to coastal production systems, with a notable contribution from the province of Guayas, and to their impact on rural employment and the trade balance. It is important to note that both fresh market performance and industrial utilisation depend fundamentally on the state of ripeness.

Despite their relevance, the postharvest chain is constrained by the climacteric behavior of the fruit. Ripening activates coordinated metabolic pathways including starch hydrolysis and sugar accumulation, cell-wall remodeling, pigment transitions, changes in bioactive compounds, and the induction of enzymatic activities associated with browning and texture loss [7]. When these processes are not adequately managed, shelf life is shortened and sensory as well as nutritional attributes deteriorate during storage, transport, and commercialization [8].

 doi:10.20944/preprints202602.2040.v1

Concurrently, consumer demand increasingly favors foods perceived as healthier and less technologically processed, which has reinforced interest in naturally ripened or well-controlled ripening processes [9]. Under this scenario, objective and operational characterization of banana quality across ripeness progression becomes essential to meet high-standard market requirements, both for fresh fruit and for processed products [10].

However, important gaps remain in the integrated characterization of physicochemical, nutritional, textural, chromatic, and enzymatic variability throughout ripening, particularly under local production conditions. Endogenous fruit factors interact with exogenous drivers (e.g., agronomic management and soil plant system conditions), potentially modulating compositional outcomes and postharvest behavior [9,11]. This systemic view treating fruit ripening as a dynamic biological process rather than a purely commercial condition has motivated monitoring and digital agriculture strategies aimed at improving both agronomic and postharvest decision-making.

From an analytical standpoint, ripening is inherently multivariate and partially nonlinear: multiple attributes co-vary and jointly define differentiated quality profiles. Consequently, integrative tools that capture covariation structures across heterogeneous variables are required. Dimensionality reduction and unsupervised learning approaches, including correlation-based interpretation and clustering, have been widely adopted for complex-system analysis [12,13]. In food research, these methods enable the identification of physiological gradients, functional associations, and parsimonious sets of discriminant variables.

In this study, we applied multivariate techniques (PCA, clustering, and multivariate hypothesis testing) to characterize Ecuadorian bananas across ripening progression using physicochemical, nutritional, chromatic, textural, and enzymatic indicators. By integrating proximal composition, carbohydrate dynamics, minerals, vitamins, instrumental color and texture, and enzymatic activity, we aimed to identify covariation patterns and functional ripening signatures that support data-driven postharvest quality management within a digital agriculture framework [14–16].

2. Materials and Methods

2.1. Study Area

The study was conducted in Milagro canton, Guayas Province, located in the coastal region of Ecuador (approximately 2°08′ S, 79°35′ W). This area is characterized by a tropical humid climate, with average annual temperatures ranging from 24 to 27 °C and relative humidity typically above 70%, conditions that favor intensive banana production and postharvest commercialization. The province of Guayas represents one of the main banana-producing regions in Ecuador, contributing significantly to national export volumes and supplying local commercial markets. Fruits used in this study were acquired from commercial distribution channels within this production area, ensuring representativeness of fruit commonly entering regional postharvest chains.

2.2. Experimental Design and Sampling

A completely randomized design was used with nine physiological stages of ripening (T1 to T9) and three biological replicates per stage (R1 to R3), for a total of 27 experimental units coded as T#R#. Each experimental unit corresponded to an independent biological replicate consisting of a pool of three fruits, processed together.

The banana fruits (Musa spp.) were obtained from a commercial batch with homogeneous initial ripeness, purchased in the Milagro canton (Guayas, Ecuador) during November and December 2025. Whole fruits were selected, with no evidence of mechanical damage, visible rot, or deformities. Transport to the laboratory was carried out in isothermal containers at 13 to 15 °C, and processing was carried out within 24 hours of acquisition in order to minimize uncontrolled postharvest changes.

Classification by maturity was performed using operational criteria based on skin coloration (Table 1). The T#R# coding was maintained in all determinations to ensure analytical traceability and comparability between replicates and stages (Ma et al., 2022).

 doi:10.20944/preprints202602.2040.v1

Table 1. Operational definition of ripening stages (T1–T9) and classification criteria.

Stage	Name	Operational criterion (peel)
T1	Deep green	Peel completely green; no visible yellowing.
T2	Green	Uniform green with slight loss of intensity.
T3	Early green–yellow	Pale green; transition stage without yellow predominance.
T4	Turning (breaker)	First visible yellow areas appear.
T5	Yellow with green tips	Predominantly yellow with residual green at the ends.
T6	Yellow	Uniform, predominantly yellow peel.
T7	Yellow with slight speckling	Yellow peel with the first brown speckles.
T8	Early overripe	Increased speckling and superficial darkening.
T9	Overripe	Evident darkening with extended blotches.

Note. The T1 to T9 scale was used as an operational classification to represent the transition of maturity (green, yellow, and overripe), maintaining the T#R# identifier throughout the entire analytical flow (Ma et al., 2022).

Plant material and analysis matrix (pulp)

Prior to classification by stages (T1 to T9), the fruits were conditioned for 24 h at 25 ± 2 °C and 70 ± 5% relative humidity, in darkness, in order to stabilize the tissue temperature and homogenize the physiological condition. Subsequently, the pulp was separated and homogenized to obtain a composite sample per experimental unit (T#R#). From the homogenized sample, aliquots were fractionated for physicochemical, compositional, mineral, vitamin, and bioactive compound determinations, which were stored at −20 °C until analysis.

Preparation of extracts

The determinations that required prior extraction were performed using aliquots of homogenized pulp corresponding to each biological replicate. The preparation of extracts was adjusted to the analytical principle of each assay (spectrophotometry or chromatography), maintaining a single consolidated value per biological replicate for subsequent statistical analysis. When repeated measurements were made within the same assay, the results were averaged to obtain a single value per biological replicate used in the statistical analysis [17,18].

Aqueous extract for free sugars (DNS

The pulp was homogenized with distilled water in a 1:10 (w/v) ratio and stirred for 30 min at 25 °C. The homogenate was centrifuged at 10,000 rpm for 10 min; the supernatant was recovered and filtered through 0.45 µm membranes. To minimize protein interference, the filtrate was deproteinized with 5% (v/v) trichloroacetic acid, centrifuged again under the same conditions, and neutralized with 1 N NaOH to pH 7.0. The extract was stored at 4 °C until analysis.

Crude extract for enzyme activity determination.

Five grams of pulp were weighed and homogenized with 10 mL of 0.1 M phosphate buffer (pH 6.5) supplemented with 1% PVP and 0.1% ascorbic acid. The mixture was stirred for 15 min at 4 °C and centrifuged at 10,000 rpm for 15 min at 4 °C. The supernatant was recovered as a crude enzyme extract and kept refrigerated until analysis.

Physicochemical and compositional determinations

Proximate composition

 doi:10.20944/preprints202602.2040.v1

The proximate composition was determined using standardized procedures for foods. The results were summarized by stage using descriptive statistics from biological replicates (Ma et al., 2022).

Total carbohydrates by difference. Total carbohydrates (CarT, %) were estimated using the difference method based on the proximal composition, according to:

$$CarT(\%) = 100 - [H + PC + GC + CT]$$

Equation (1). Calculation of total carbohydrates by difference.

In Equation (1), H corresponds to moisture (%), PC to crude protein (%), GC to crude fat (%), and CT to total ash (%). All variables were expressed as percentage (%).

2.5.2. Determination of Minerals (K, Mg, Ca, and Zn)

The minerals K, Mg, Ca, and Zn were quantified after wet digestion of the plant matrix in nitric acid, followed by instrumental reading for elemental analysis. Sample preparation was based on established procedures for plant material aimed at multi-element determinations (Zarcinas et al., 1987). Potassium (K) was determined by flame photometry, with calibration using standard solutions [19]. Mg, Ca, and Zn were quantified by flame atomic absorption spectrophotometry (FAAS) in a Z-2000 Tandem Flame/Furnace AA Spectrophotometer (Hitachi, Japan), using an acetylene-air flame and Zeeman background correction. The wavelengths were 285.2 nm for Mg, 422.7 nm for Ca, and 213.9 nm for Zn. To minimize interference from phosphates in Ca and Mg, 1% $LaCl_3$ was used as a releasing agent. Quantification was performed using an external calibration curve. The results were expressed in mg kg^{-1} [20].

2.5.3. Determination of Bioactive Compounds (Oxalic Acid and Total Tannins)

Oxalic acid (OA) and total tannins (TA), expressed as tannic acid equivalents, were quantified as bioactive variables for comparison between stages of ripening. The determination was performed using validated analytical procedures for organic acids and phenolic compounds in plant matrices, reporting a value per biological replicate (T#R#) and its summary per stage (Ma et al., 2022). The results were expressed in μg g^{-1}.

2.5.4. Enzymatic Activity Associated with Browning (PPO and POD)

Polyphenol oxidase (PPO) activity was determined in crude extract using 0.05 M Tris-HCl buffer (pH 7.0) and 0.2 M pyrocatechol as substrate. The reaction mixture was prepared with 2.6 mL of substrate and 0.1 mL of enzyme extract, recording the increase in absorbance at 390 nm at 1-minute intervals. Activity was expressed as the change in absorbance per minute normalized by tissue mass and reported by stage from biological replicates [21].

Peroxidase (POD) activity was evaluated in crude extract prepared in 0.2 M sodium phosphate buffer (pH 6.0) with 5% NaCl. The substrate solution was prepared in 0.2 M sodium phosphate buffer with 0.05 M guaiacol and 0.02 M H_2O_2. The reaction mixture consisted of 2.9 mL of substrate solution and 0.1 mL of enzyme extract, recording the increase in absorbance at 420 nm per minute. Activity was expressed as the variation in absorbance per minute normalized by tissue mass and reported per stage from biological replicates [22].

2.5.5. Color (CIELAB) and Instrumental Texture

The color of the skin and flesh was determined using a CM-5 spectrophotometer (Konica Minolta, Tokyo, Japan) employing the CIELAB space (L*, a*, b*) based on instrumental reflectance measurements (Ma et al., 2022). Illuminant D65 and a 10° observer were used, with d/8 measurement geometry in an integrating sphere. Five readings were taken at random points per experimental unit on the skin; on the pulp, readings were taken on the exposed cut surface. The values per experimental

 doi:10.20944/preprints202602.2040.v1

unit were obtained as the average of the readings and were consolidated by stage for comparative ripening analysis (Ma et al., 2022).

The pulp texture was evaluated in a TA-XT2 texturometer (Stable Micro Systems, UK) with a P/10 cylindrical probe (10 mm in diameter). The test was performed with a pre-test speed of 3 mm s^{-1}, a test speed of 1 mm s^{-1}, and a post-test speed of 1 mm s^{-1}, applying a 50% deformation to the sample. For each experimental unit, determinations were made in triplicate and the results were consolidated as an average per biological replicate (Ma et al., 2013).

2.6. Quantification of Starch and Sugars

2.6.1. Total Starch (TS)

Total starch (TS, %) was quantified by sequential enzymatic hydrolysis with α-amylase and amyloglucosidase for conversion to glucose, followed by colorimetric quantification (GOPOD type) and calibration with a glucose standard. The results were expressed as a percentage and reported by stage based on biological replicates [17].

Quantification was obtained using the following expression:

$$TS(\%) = \frac{(\Delta E \times F)}{(W \times FV \times 0.9)}$$

Equation (2). Calculation of total starch.

In Equation (2), ΔE represents the absorbance of the sample relative to the blank, F is the conversion factor derived from the standard, W is the sample mass (mg), FV corresponds to the final volume of the extract, and 0.9 is the stoichiometric conversion factor from glucose to starch (162/180).

2.6.2. Resistant Starch (RS)

Resistant starch (RS, %) was determined by differential enzymatic digestion and colorimetric reading, following validated procedures for its measurement in plant matrices [24]. The concentration was calculated from the absorbance of the sample relative to the blank (ΔE), using:

$$RS(\%) = \frac{(\Delta E \times F)}{(W \times 9.27)}$$

Equation (3). Calculation of resistant starch.

In Equation (3), ΔE is the absorbance relative to the blank, F is the conversion factor, W is the sample mass (mg), and 9.27 corresponds to the applied overall volumetric correction factor.

2.6.3. Free Sugars (FS) (DNS)

Free sugars were quantified using the 3,5-dinitrosalicylic acid (DNS) method with spectrophotometric reading (Miller, 1959). 0.5 mL of the sample extract was mixed with 0.5 mL of DNS reagent; the mixture was heated to boiling for 10 min, cooled to room temperature, and 5 mL of distilled water was added. Absorbance was measured at 540 nm and quantification was performed using an external calibration curve with glucose standard. The results were expressed in g 100 g^{-1} of pulp and reported by stage from biological replicates [18].

2.7. Total Soluble Solids (°Brix)

Total soluble solids (°Brix) were determined using an Atago PAL-1 handheld refractometer (0–53 °Brix), previously calibrated with distilled water. Readings were taken on the filtrate of the aqueous pulp extract and recorded once the value had stabilized. When repeated readings were taken

 doi:10.20944/preprints202602.2040.v1

per sample, the values were averaged to obtain a single value per biological replicate (T#R#). The results were reported per stage as mean ± standard deviation (n = 3) [25,26].

2.8. pH Measurement

The pH was determined per biological replicate (T#R#) using a potentiometer with a glass electrode, previously calibrated with traceable buffer solutions (pH 4.00 and 7.00; and pH 10.01 when applicable), with temperature compensation at 25 ± 1 °C. The pH was measured in an aqueous extract prepared from homogenized pulp; 10 g of pulp was mixed with 10 mL of distilled water (1:1, m/m), homogenized for 1 min, and the supernatant was filtered before reading. For repeated measurements per sample, the values were averaged to obtain a single value per replicate. Results were reported per stage as mean ± standard deviation (n = 3) ISO 1842: , [27,28].

2.9. Titratable Acidity

Titratable acidity (TA) was determined by acid-base titration with NaOH to the endpoint indicated by phenolphthalein, and expressed as a percentage of the reference acid of the method (malic acid). The calculation was performed in accordance with standard NTE INEN-ISO 750: , [29], using Equation (4). The results were obtained by biological replication (T#R#) and reported by stage as mean ± standard deviation (n = 3).

$$Titratable\ acidity \quad = \frac{(67.045)}{(V)} \times V_1 \times C \times \frac{(100)}{(V_0)}$$

Equation (4). Calculation of titratable acidity.

In Equation (4), V represents the volume of the test sample (mL), V_0 corresponds to the volume of the titrated portion (mL), V_1 is the volume of NaOH consumed (mL), 67.045 is the equivalent weight of malic acid (g·eq^{-1}), and C is the concentration of NaOH (mol L^{-1}).

2.10. Determination of Vitamins by HPLC

Vitamin C (C; µg g^{-1}) was quantified by high-performance liquid chromatography (HPLC) with UV detection, following validated procedures for plant matrices (Alós et al., 2015). A Thermo Scientific Vanquish Core HPLC system equipped with a Mightysil RP-18 column (4.0 × 250 mm, 5 µm; Kanto Chemical) was used. The mobile phase consisted of 0.05 M KH_2PO_4 (pH 4.6) and acetonitrile in a 30:70 (v/v) ratio, with a flow rate of 1.0 mL min^{-1}, injection volume of 20 µL, and detection at 210 nm. The samples were prepared according to the extraction procedure described above and filtered with a 0.45 µm membrane before analysis. Quantification was performed by external calibration with ascorbic acid standard and the results were reported in µg g^{-1} [30].

Vitamins B1 (thiamine) and B6 (pyridoxine), expressed in µg g^{-1}, were determined by HPLC with fluorescence detection according to validated chromatographic schemes, including preparation of extracts compatible with the stability of water-soluble vitamins [31].

2.11. Synthesis of Variables and Analytical Methods

Based on the objective of the study, quantitative variables representative of the physicochemical, nutritional, and bioactive profile of the fruit were considered, grouped into analytical blocks: carbohydrates/sugars, proximate composition, minerals, vitamins, bioactive compounds, enzymatic activity, and instrumental parameters. Table 2 summarizes the coding of variables, reporting units, and corresponding analytical technique.

 doi:10.20944/preprints202602.2040.v1

Table 2. Analytical variables, reporting units, and determination technique.

Block	Variables (codes)	Unit	Technique / principle
Carbohydrates	TS, RS	%	Enzymatic digestion and colorimetric quantification
Sugars	FS	g 100 g^{-1}	DNS with UV-Vis reading (540 nm)
Proximate composition	H, PC, GC, CT, FC, CarT	%	Standard proximate determinations; CarT by difference
Minerals	K, Mg, Ca, Zn	mg kg^{-1}	Acid digestion and elemental reading (flame photometry for K; FAAS for Mg, Ca, and Zn)
Vitamins	C, B1, B6	μg g^{-1}	HPLC (UV for C; fluorescence for B1 and B6)
Bioactives	OA, TnA	μg g^{-1}	Validated procedures for organic acids and tannins
Enzymes	PPO, POD	U g^{-1}	UV-Vis kinetic assays (390 nm for PPO; 420 nm for POD)
Color	L*, a*, b*	dimensionless	Reflectance spectrophotometry (CIELAB)
Texture	Fmax (and associated metrics)	N (and variable-dependent units)	Mechanical test in a texture analyzer (force–deformation profile)

Note. Results were consolidated at the biological replicate level (T#R#). TS and RS were expressed as %, AL as g 100 g^{-1}, minerals as mg kg^{-1}, and vitamins and bioactives as μg g^{-1}. CarT was estimated by difference from the proximal composition. PPO and POD were reported as enzyme activities derived from UV-Vis kinetic assays [17–24].

2.12. Statistical Analysis

Monotonic associations between variables were evaluated using Spearman's correlation, with a significance level of $p < 0.05$. The analyses were performed in R (version 4.5.0; R Foundation for Statistical Computing) using Rstudio IDE (v2025.09.2), using the vegan, FactoMineR, ggplot2, factoextra, corrplot, and tidyverse packages.

Overall differences between stages were evaluated using PERMANOVA on distance matrices, considering the stage as a fixed factor. Significance was determined based on the pseudo-F statistic, the coefficient of determination (R^2), and p-values obtained by permutations [32].

The multivariate variation structure was explored using PCA applied to standardized data, interpreting explained variance, loadings, and biplots [12,13,33]. Additionally, unsupervised

 doi:10.20944/preprints202602.2040.v1

clustering using k-means (k = 9) was applied as an exploratory analysis to evaluate the consistency of replicates and differentiation between stages.

3. Results

3.1. Data Structure and Verification of Statistical Assumptions

Banana fruits (Musa spp.) classified into nine physiological stages of ripeness (T1–T9) were analyzed. For each stage, three independent biological replicates (n = 27) were included, and the results were summarized at the stage level as mean ± standard deviation (SD), according to the experimental design described in the Methodology and Annexes section.

The evaluation of assumptions was performed on the complete set of observations (27 experimental units) to determine the adequacy of parametric procedures and the need for transformations/standardization. Deviation from normality was observed in most variables ($p < 0.05$). This trend was most evident in indicators related to carbohydrate hydrolysis (total starch, resistant starch, and soluble solids), instrumental texture parameters (maximum force, modulus, cohesiveness, and adhesiveness), color attributes of the shell, and enzymatic activities associated with browning (polyphenol oxidase and peroxidase).

In contrast, a subset of variables showed a distribution compatible with normality ($p \geq 0.05$), including minerals (K, Mg, Ca, and Zn), B vitamins (B1 and B6), and some color and proximal composition attributes. Given the coexistence of variables with different distributional behavior, the results were summarized by stage using descriptive statistics (mean ± SD) and, for multivariate analyses, the variables were standardized beforehand to ensure comparability between scales and avoid the dominance of those with greater magnitude.

3.2. Carbohydrates and Soluble Solids During Ripening

Total starch (TS) showed a uniform decrease throughout the nine stages of ripening, consistent with the consumption of starchy reserves in early stages. Maximum values were recorded in T1 (22.76 ± 0.13%), followed by a gradual reduction in T2–T3 and a more marked drop from T4 onwards. By T5, TS reached 13.03 ± 0.20%, and minimum values (4.28 ± 0.11%) were observed in T9. In relative terms, the cumulative decrease between T1 and T9 was approximately 81.2%, with low intra-stage variability, supporting the consistency of the biological replicates.

Resistant starch (RS) showed a pattern consistent with RT, with a sustained reduction from 10.60 ± 0.05% (T1) to 4.98 ± 0.10% (T5) and 1.41 ± 0.04% (T9). The observed range (1.41–10.60%) corresponds to an approximate relative decrease of 86.7% between the beginning and end of ripening. The reduced standard deviations suggest high reproducibility between replicates within each stage.

Concomitantly, free sugars (FS) and soluble solids (°Brix) showed a progressive increase throughout the process. °Brix increased from 5.11 ± 0.10 (T1) to 13.81 ± 0.10 (T5), reaching a maximum of 22.00 ± 0.26 (T9), representing an approximate cumulative increase of 330%. This behavior is consistent with starch hydrolysis and the accumulation of soluble sugars, a central phenomenon in the climacteric ripening of bananas.

Table 3. Carbohydrate and soluble solids profile by stage (mean ± SD, n = 3).

Stage	TS (Total starch, %)	RS (Resistant starch, %)	FS (Free sugars, %)	Soluble solids (°Brix)
T1	22.76 ± 0.13	10.60 ± 0.05	2.05 ± 0.19	5.11 ± 0.10
T2	20.55 ± 0.22	9.42 ± 0.10	2.59 ± 0.16	6.16 ± 0.09
T3	18.23 ± 0.23	7.94 ± 0.20	4.17 ± 0.36	8.22 ± 0.11

 doi:10.20944/preprints202602.2040.v1

T4	15.72 ± 0.34	6.44 ± 0.11	6.72 ± 0.13	11.20 ± 0.06
T5	13.03 ± 0.20	4.98 ± 0.10	9.93 ± 0.09	13.81 ± 0.10
T6	10.52 ± 0.14	3.83 ± 0.06	12.65 ± 0.11	16.36 ± 0.09
T7	7.91 ± 0.21	2.87 ± 0.14	15.68 ± 0.30	18.73 ± 0.06
T8	5.92 ± 0.15	1.99 ± 0.05	18.41 ± 0.23	20.96 ± 0.20
T9	4.28 ± 0.11	1.41 ± 0.04	20.38 ± 0.31	22.00 ± 0.26

Note. A pattern consistent with ripening is observed, in which TA and RA decrease due to the mobilization and degradation of starchy reserves, while LA and soluble solids (°Brix) increase due to the accumulation of soluble sugars derived from this conversion.

3.3. Proximal Composition Evolution

Moisture increased progressively throughout maturation, from 74.07 ± 0.11% (T1) to 76.37 ± 0.10% (T5) and 79.72 ± 0.06% (T9), corresponding to an approximate relative increase of 7.63% between the extreme stages. This behavior suggests a higher proportion of aqueous fraction as maturation progresses.

Crude protein showed a downward trend, with values of 1.341 ± 0.016% (T1), 1.198 ± 0.010% (T5), and 1.064 ± 0.020% (T9). Crude fat remained at low levels, with limited variation between stages (0.348 ± 0.001% in T1 versus 0.276 ± 0.008% in T9), indicating relative stability of this fraction in the evaluated interval.

Similarly, total carbohydrates decreased from 23.35 ± 0.11% (T1) to 18.07 ± 0.07% (T9) (−22.6%), while crude fiber showed a sustained reduction from 2.672 ± 0.024% to 1.833 ± 0.000% (−31.4%). The simultaneous decrease in carbohydrates and fiber is consistent with structural changes in the tissue during ripening, including the remodeling of cell wall components and the conversion of reserves into soluble fractions.

Table 4. Proximal composition by stage of ripening (mean ± SD; n = 3).

Stage	Moisture (%)	Crude protein (%)	Crude fat (%)	Total ash (%)	Total carbohydrates (%)	Crude fiber (%)
T1	74.07 ± 0.11	1.341 ± 0.017	0.348 ± 0.001	0.895 ± 0.006	23.35 ± 0.11	2.673 ± 0.024
T2	74.26 ± 0.07	1.338 ± 0.033	0.339 ± 0.009	0.880 ± 0.004	23.20 ± 0.07	2.611 ± 0.012
T3	74.88 ± 0.05	1.282 ± 0.009	0.337 ± 0.004	0.877 ± 0.004	22.60 ± 0.19	2.543 ± 0.015
T4	75.53 ± 0.09	1.238 ± 0.009	0.323 ± 0.006	0.870 ± 0.006	22.00 ± 0.11	2.457 ± 0.015
T5	76.37 ± 0.10	1.198 ± 0.010	0.317 ± 0.003	0.852 ± 0.005	21.32 ± 0.10	2.306 ± 0.010
T6	77.03 ± 0.06	1.154 ± 0.012	0.307 ± 0.004	0.840 ± 0.006	20.63 ± 0.07	2.217 ± 0.010
T7	78.06 ± 0.06	1.121 ± 0.014	0.296 ± 0.004	0.830 ± 0.006	19.50 ± 0.07	2.086 ± 0.006
T8	78.92 ± 0.05	1.091 ± 0.013	0.289 ± 0.004	0.824 ± 0.005	18.77 ± 0.08	1.948 ± 0.009
T9	79.72 ± 0.06	1.064 ± 0.020	0.276 ± 0.008	0.817 ± 0.004	18.07 ± 0.07	1.833 ± 0.000

Note. Moisture increases monotonically (T1→T9), while total carbohydrates (CarT) and crude fiber (CF) decrease, suggesting a compositional reconfiguration of the fruit matrix as ripening progresses.

 doi:10.20944/preprints202602.2040.v1

3.4. Variation in Minerals (K, Mg, Ca, and Zn)

Potassium (K) was the predominant mineral at all stages of ripening and, although it maintained high concentrations, it showed a downward trend from T1 to T9. At T1, 4091.67 ± 34.14 mg kg^{-1} was recorded, decreasing to 3900.57 ± 11.97 mg kg^{-1} at T5 and to 3713.13 ± 23.36 mg kg^{-1} at T9. The observed range (3713.13–4091.67 mg kg^{-1}) corresponds to an approximate relative reduction of 9.25% between extreme stages.

Magnesium (Mg) showed proportional behavior, with values between 279.73 ± 2.93 mg kg^{-1} (T1) and 255.30 ± 1.68 mg kg^{-1} (T9), and an intermediate value of 268.57 ± 0.51 mg kg^{-1} (T5), equivalent to an approximate relative decrease of 8.73% during ripening. Similarly, calcium (Ca) decreased from 65.13 ± 1.13 mg kg^{-1} (T1) to 60.43 ± 0.30 mg kg^{-1}

(T5) and 57.64 ± 0.60 mg kg^{-1} (T9), representing a total reduction of approximately 11.5%.

Zinc (Zn) remained at low and relatively stable concentrations, with values of 3.19 ± 0.07 mg kg^{-1} (T1), 3.01 ± 0.04 mg kg^{-1} (T5), and 2.78 ± 0.03 mg kg^{-1} (T9), corresponding to an approximate relative reduction of 12.7%. Overall, intra-stage dispersion was low to moderate, according to the standard deviations observed.

Table 5. Mineral content by stage of maturation (mean ± SD; n = 3).

Stage	Potassium, K	Magnesium, Mg	Calcium, Ca	Zinc, Zn
T1	4091.67 ± 34.14	279.73 ± 2.93	65.13 ± 1.13	3.19 ± 0.07
T2	4011.07 ± 8.19	275.73 ± 3.19	64.00 ± 0.91	3.12 ± 0.06
T3	3960.70 ± 7.75	272.47 ± 1.96	63.20 ± 0.44	3.09 ± 0.06
T4	3925.20 ± 15.49	270.43 ± 0.81	61.70 ± 0.35	3.05 ± 0.05
T5	3900.57 ± 11.97	268.57 ± 0.51	60.43 ± 0.30	3.01 ± 0.04
T6	3843.23 ± 4.61	263.70 ± 1.51	59.53 ± 0.40	2.95 ± 0.04
T7	3808.63 ± 30.94	260.67 ± 0.92	58.67 ± 0.31	2.88 ± 0.04
T8	3759.63 ± 18.02	257.83 ± 0.86	58.20 ± 0.36	2.83 ± 0.04
T9	3713.13 ± 23.36	255.30 ± 1.68	57.64 ± 0.60	2.78 ± 0.03

Note. K, Mg, Ca, and Zn show moderate decreases toward late stages of ripening; the limited standard deviations suggest limited intra-stage variability (intra-phase stability) in mineral concentrations.

Vitamin C exhibited a non-monotonic pattern throughout ripening, with an increase from 92.33 ± 0.74 μg g^{-1} (T1) to a maximum in the intermediate stage (110.17 ± 2.35 μg g^{-1} at T5), followed by a decrease towards the late stages (81.60 ± 1.74 μg g^{-1} at T9). The observed range (81.60–110.17 μg g^{-1}) indicates a transient peak in the intermediate phase, consistent with a dynamic balance between accumulation and loss (e.g., oxidation) of ascorbic acid as ripening progresses.

Vitamin B1 (thiamine) remained within a narrow range, with values of 0.447 ± 0.006 μg g^{-1} (T1), a slight increase to 0.493 ± 0.012 μg g^{-1} (T5) and 0.454 ± 0.006 μg g^{-1} (T9), suggesting limited variations between stages. In parallel, vitamin B6 showed moderate variation: it increased from 0.693 ± 0.006 μg g^{-1} (T1) to 0.777 ± 0.021 μg g^{-1} (T5) and decreased slightly to 0.713 ± 0.015 μg g^{-1} (T9) (range: 0.693–0.777 μg g^{-1}). Compared to B1, B6 showed a greater range of change throughout the ripening gradient.

 doi:10.20944/preprints202602.2040.v1

Table 6. Vitamins by ripening stage (mean ± SD; n = 3).M.

Stage	Vitamin C	Vitamin B1	Vitamin B6
T1	92.33 ± 0.74	0.447 ± 0.006	0.693 ± 0.006
T2	95.63 ± 1.36	0.461 ± 0.009	0.717 ± 0.012
T3	99.87 ± 1.05	0.469 ± 0.010	0.733 ± 0.015
T4	104.77 ± 1.02	0.477 ± 0.012	0.757 ± 0.015
T5	110.17 ± 2.35	0.493 ± 0.012	0.777 ± 0.021
T6	103.53 ± 1.37	0.485 ± 0.010	0.760 ± 0.020
T7	97.10 ± 1.11	0.471 ± 0.010	0.747 ± 0.015
T8	89.67 ± 1.36	0.464 ± 0.009	0.733 ± 0.015
T9	81.60 ± 1.74	0.454 ± 0.006	0.713 ± 0.015

Note. Vitamin C peaks at the intermediate stage (T5) and decreases in the late stages, while vitamins B1 and B6 remain within narrow ranges, with a more marked variation for B6.

3.6. Color Evolution (CIELAB) in Peel and Pulp

In the peel, the L* parameter showed a sustained increase throughout the ripening gradient, going from 44.94 ± 0. 27 (T1) to 59.94 ± 0.53 (T5) and 62.16 ± 0.90 (T9), with an overall range of 44.94–62.16, indicating an increase in surface brightness as the fruit ripens.

On the other hand, the a* parameter showed a marked transition from negative values in the early stages (−12.01 ± 0.38 at T1) to values close to zero in the intermediate stages (−0.17 ± 0.09 at T5) and positive values in the advanced stages (7.15 ± 0.21 at T9), consistent with the chromatic shift from the green → red axis.

Complementarily, the b* parameter increased continuously from 22.15 ± 0.31 (T1) to 45.14 ± 0.54 (T5) and 50.09 ± 0.81 (T9) (range: 22.15–50. 09), reflecting the increase in the yellow component characteristic of mature states. In the pulp, the chromatic variations were smaller in magnitude; however, the general trends were consistent with those observed in the peel, especially from the intermediate and late stages onwards.

Table 7. CIELAB parameters in the peel by stage of ripeness (mean ± SD; n = 3).

Stage	Skin L*	Skin a*	Skin b*
T1	44.94 ± 0.27	-12.01 ± 0.38	22.15 ± 0.31
T2	46.97 ± 0.41	-9.29 ± 0.23	25.15 ± 0.23
T3	47.06 ± 0.04	-7.29 ± 0.19	29.29 ± 0.41
T4	54.64 ± 0.17	-2.95 ± 0.17	38.15 ± 0.36
T5	59.94 ± 0.53	-0.17 ± 0.09	45.14 ± 0.54
T6	60.46 ± 0.35	1.41 ± 0.10	46.75 ± 0.43
T7	61.10 ± 0.38	3.65 ± 0.11	47.97 ± 0.32
T8	61.68 ± 0.55	5.56 ± 0.14	49.15 ± 0.38

 doi:10.20944/preprints202602.2040.v1

Stage	Skin L*	Skin a*	Skin b*
T9	62.16 ± 0.90	7.15 ± 0.21	50.09 ± 0.81

Note. In the skin, L* increases (greater brightness), a* shifts from negative to positive values (green→red transition), and b* increases (greater yellowness) as ripening progresses.

3.7. Evolution of Instrumental Texture

The instrumental texture parameters showed a sustained softening of the tissue throughout maturation (Table 8). The maximum force (Fmax) decreased from 39.73 ± 0.74 N (T1) to 18.16 ± 0.46 N (T5) and 5.43 ± 0.10 N (T9), which is equivalent to an approximate cumulative reduction of 86.3% between the extreme stages. Similarly, the modulus showed a marked decline from 20085 ± 329 Pa (T1) to 7987 ± 35 Pa (T5) and 2105 ± 280 Pa (T9) (range: 2105–20085 Pa), reflecting a pronounced loss of structural rigidity as the process progresses.

Cohesiveness showed a gradual decrease from 0.617 ± 0.003 (T1) to 0.560 ± 0.003 (T5) and 0.450 ± 0.010 (T9) (relative reduction ≈ 27.1%), consistent with lower mechanical integrity of the tissue in late stages. In contrast, adhesiveness increased from 0.053 ± 0.007 (T1) to 0.117 ± 0.003 (T5) and 0.250 ± 0.000 (T9), representing an approximate increase of 372%, indicating greater adhesiveness/stickiness in advanced stages of maturity.

Overall, the standard deviations suggest limited intra-stage variability for cohesiveness and adhesiveness, and moderate variability for modulus, particularly at T9.

Table 8. Instrumental texture by stage of ripeness (mean ± SD; n = 3).

Stage	Fmax (N)	Modulus (Pa)	Cohesiveness	Adhesiveness
T1	39.73 ± 0.74	20085 ± 329	0.617 ± 0.003	0.053 ± 0.007
T2	36.13 ± 0.46	17754 ± 199	0.606 ± 0.006	0.064 ± 0.006
T3	29.95 ± 0.70	15018 ± 39	0.593 ± 0.008	0.078 ± 0.005
T4	24.44 ± 0.25	10546 ± 69	0.576 ± 0.007	0.095 ± 0.001
T5	18.16 ± 0.46	7987 ± 35	0.560 ± 0.003	0.117 ± 0.003
T6	13.53 ± 0.49	6077 ± 51	0.534 ± 0.004	0.144 ± 0.003
T7	9.44 ± 0.24	3846 ± 94	0.503 ± 0.005	0.183 ± 0.004
T8	7.03 ± 0.14	2824 ± 96	0.474 ± 0.006	0.217 ± 0.006
T9	5.43 ± 0.10	2105 ± 280	0.450 ± 0.010	0.250 ± 0.000

Note. Fmax and modulus decrease from T1 to T9 (softening), cohesiveness decreases, and adhesiveness increases towards advanced stages.

3.8. Enzymatic Activity: PPO and POD

Polyphenol oxidase (PPO) activity showed a sustained increase throughout the nine stages of ripening, from 19.90 ± 0.34 (T1) to 37.84 ± 0.29 (T5) and 55.87 ± 0.21 (T9) (range: 19.90–55. 87). This behavior corresponds to an approximate relative increase of 180.8% between the extreme stages (Table 9).

Consistently, peroxidase (POD) increased from 14.86 ± 0.83 (T1) to 28.34 ± 0.89 (T5) and 47.54 ± 0.83 (T9) (range: 14.86–47. 54), representing an approximate relative increase of 219.9%. Overall, both enzymes showed an upward trend consistent with the progress of ripening.

 doi:10.20944/preprints202602.2040.v1

The limited standard deviations at most stages suggest limited intra-stage variability in enzyme measurements.

Table 9. Enzyme activity by ripening stage (mean ± SD; n = 3).

Stage	PPO (U g^{-1})	POD (U g^{-1})
T1	19.90 ± 0.34	14.86 ± 0.83
T2	21.76 ± 0.54	17.54 ± 0.38
T3	24.27 ± 0.82	20.19 ± 0.22
T4	30.63 ± 0.45	23.45 ± 0.84
T5	37.84 ± 0.29	28.34 ± 0.89
T6	43.14 ± 0.46	33.16 ± 0.76
T7	48.02 ± 0.22	38.67 ± 0.47
T8	52.12 ± 0.33	43.11 ± 0.57
T9	55.87 ± 0.21	47.54 ± 0.83

Note. PPO and POD show sustained increases from T1 to T9, displaying a pattern consistent with the progress of ripening.

3.9. Multivariate Analysis of Physicochemical and Nutritional Variation During Ripening: PERMANOVA and Multivariate Ordination Analysis (PCA)

Permutational multivariate analysis of variance (PERMANOVA) (Table 10) revealed significant multivariate differences between the nine stages of ripening (pseudo-F = 2758.3; p = 0.001). The value of R^2 = 0.99918 suggests that, under the distance matrix used, the ripening stage explains practically all of the multivariate variation observed, while the residual variation associated with differences between replicates within the stage was comparatively low (residual R^2 = 0.00082).

The model was adjusted on a multivariate distance matrix and formulated as:

$$multivariate\ distance\ \sim\ stage\ of\ ripeness$$

Table 10. PERMANOVA results for multivariate variation between stages of banana ripeness.

	Df	SumOfSqs	R^2	F	Pr(>F)
Model	8	1052875109	0.99918	2758.3	0.001 ***
Residual	18	858865	0.00082		
Total	26	1053733975	100.000		

In the Table 10, permutational multivariate analysis of variance (PERMANOVA) revealed significant multivariate differences between ripening stages (pseudo-F = 2758.3; R^2 = 0.999; p = 0.001), indicating a strong separation among maturity levels within the multivariate space. The very high R^2 value reflects the controlled experimental design and the clear physiological differentiation among predefined ripening stages. Therefore, this result should be interpreted within the context of standardized experimental conditions rather than as a representation of natural variability under field or commercial scenarios.

 doi:10.20944/preprints202602.2040.v1

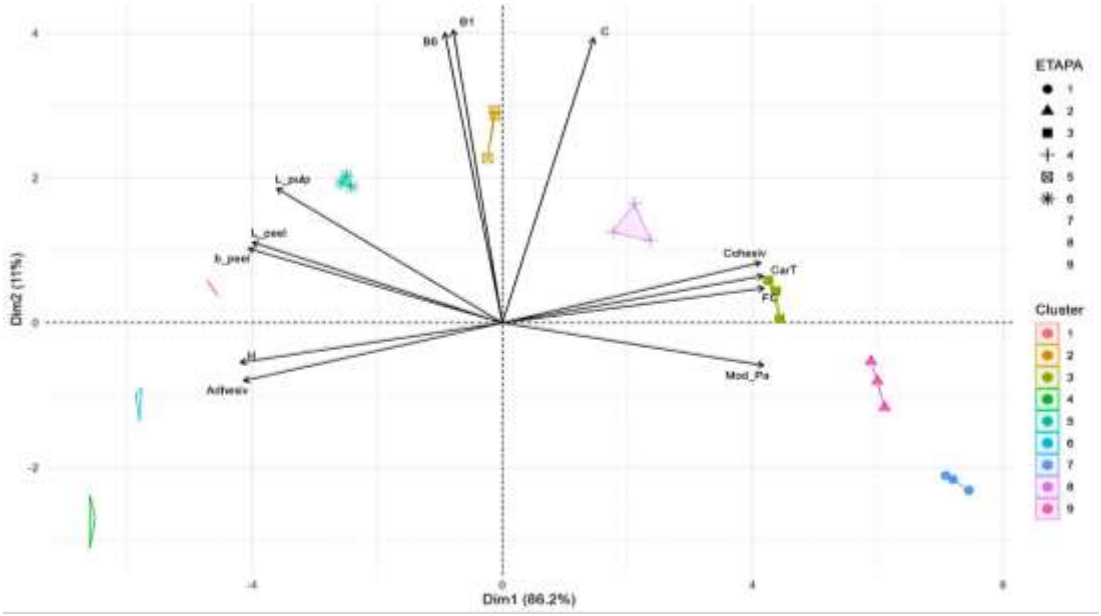

Figure 1. Biplot of Principal Component Analysis (PCA) showing the distribution of banana ripening stages (T1–T9) and the contribution of physicochemical, nutritional, chromatic, texture, and enzymatic activity variables.

Additionally, principal component analysis (PCA; Figure 1), applied to 29 variables standardized using Z-scores (carbohydrates and sugars, proximate composition, minerals, vitamins, color, texture, and enzyme activity), explained 97.2% of the total variation across the first two dimensions (Dim1 = 86.2%; Dim2 = 11.0%), defining a well-structured multivariate maturation gradient. The projection of the biological replicates showed a consistent separation by stage; complementarily, the k-means clustering (k = 9) assigned the three replicates of each stage to the same cluster in a concordant manner, suggesting low intra-stage dispersion and a marked differentiation between stages in the multivariate space.

The early stages (T1–T3) were concentrated at the positive end of Dim1, characterized by higher total and resistant starch (AT, AR) contents, higher firmness (Fmax) and modulus, as well as higher values of crude fiber (CF), total carbohydrates (CarT), crude protein (CP), and minerals (K, Mg, Ca, and Zn). The advanced stages (T7–T9) were located at the negative end of Dim1, associated with an increase in free sugars (FS) and soluble solids (°Brix), higher moisture content (M), color shifts in the skin and pulp (increase in a* and b*), higher PPO and POD activities, and increased adhesiveness. Taken together, this organization suggests a coordinated transition from a profile dominated by starchy reserves and tissue structure to a profile dominated by carbohydrate solubilization, tissue softening, and increased oxidative components during ripening.

Dim2 captured variation of lesser magnitude, mainly associated with vitamins (C, B1, and B6) and lightness (L*), allowing for more accurate discrimination of the intermediate stages with respect to the extremes of the gradient. The interpretation of the biplot indicated direct associations between variables with close and aligned vectors, while opposite orientations reflected inverse relationships, particularly between AT and AR versus AL, °Brix, and enzyme activity.

 doi:10.20944/preprints202602.2040.v1

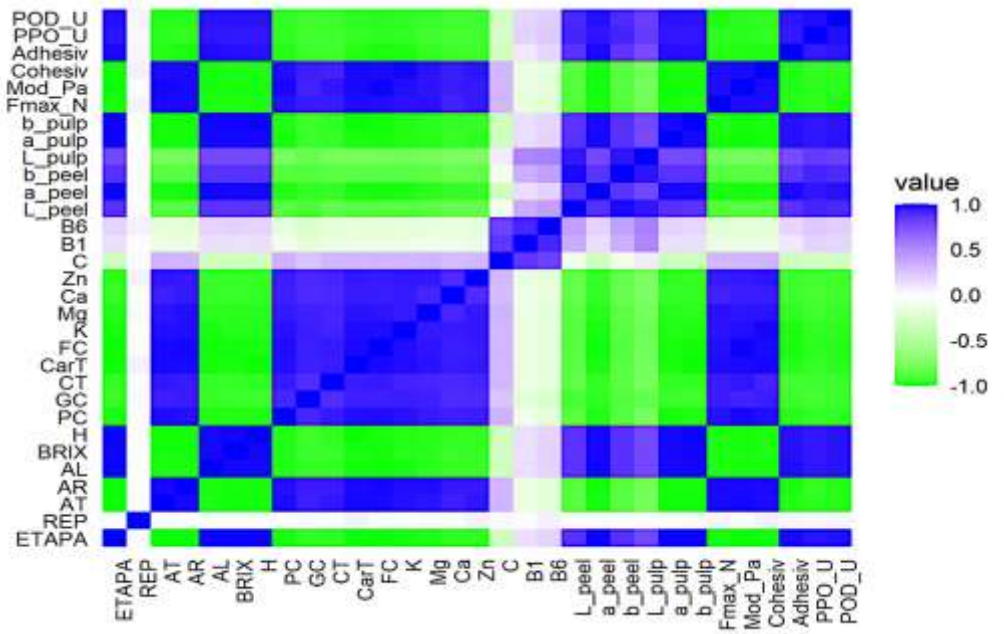

Figure 2. Spearman correlation matrix between physicochemical, nutritional, textural, chromatic, and enzymatic variables of bananas during the ripening stages (T1–T9). The colors indicate the direction and intensity of the monotonic correlation (ϱ), from strong negative correlations (green) to strong positive correlations (blue).

The Spearman correlation matrix (Figure 2) showed robust monotonic associations between the main indicators of ripening. Stage progression (T1→T9) was negatively correlated with total starch (TS) and resistant starch (RS) ($\varrho \approx -0.99$; $p < 0.001$), as well as with firmness attributes (Fmax and modulus) ($\varrho \approx -0.99$; $p < 0.001$). In contrast, stage was positively associated with free sugars (FS) and soluble solids (°Brix) ($\varrho \approx 0.99$; $p < 0.001$), with adhesiveness ($\varrho \approx 0.99$; $p < 0.001$), and with PPO and POD activity ($\varrho \approx 0.97$–0.98; $p < 0.001$), supporting a coordinated transition toward a more soluble, less firm profile with greater potential for enzymatic reaction in late stages.

In bivariate relationships, AL and °Brix showed a very high positive correlation ($\varrho \approx 0.99$), while both were inversely associated with AT/AR ($\varrho \approx -0.98$ to -0.99). Consistently, adhesiveness was negatively related to Fmax and modulus ($\varrho \approx -0.97$ to -0.98), reinforcing the co-occurrence of softening and increased tissue adhesiveness during ripening.

In addition, PPO and POD were closely correlated with each other ($\varrho \approx 0.98$) and showed a positive association with color change toward higher a* values in the peel ($\varrho \approx 0.96$), in line with their joint contribution to oxidative processes associated with browning in advanced stages. Finally, minerals (e.g., K–Mg; Ca–Zn) and components of the proximal composition tended to correlate positively with each other and to cluster together with firmness indices, in opposition to the block formed by soluble sugars, adhesiveness, and enzymatic activities.

4. Discussion

4.1. Main Axis of Ripening

This multivariate structure is supported by PERMANOVA (pseudo-F = 2758.3; $R^2 = 0.999$), indicating that ripening stage accounted for the dominant fraction of variation under the selected distance matrix, with comparatively low intra-stage dispersion. Although the explained variation was exceptionally high, this outcome is consistent with the controlled experimental design and the predefined classification of ripening stages, where strong physiological differentiation is expected under standardized conditions. Therefore, the high explanatory power should be interpreted within the context of experimentally defined stages rather than natural commercial variability.

 doi:10.20944/preprints202602.2040.v1

Although stage classification was operationally based on peel coloration, the multivariate organization demonstrates that visual stages correspond to coordinated internal biochemical and structural transitions rather than isolated external traits. This pattern is consistent with the climacteric nature of Musa spp., in which ethylene signaling regulates transcriptional and metabolic processes associated with reserve mobilization, tissue softening, and pigment transformation [34]. Similar multivariate ripening gradients have been reported in Cavendish bananas under different production conditions, supporting the interpretation of ripening as a continuous physiological process rather than a sequence of isolated events. However, the present study extends previous approaches by integrating physicochemical, nutritional, textural, chromatic, and enzymatic variables within a unified multivariate framework, enabling a more comprehensive characterization of ripening dynamics.

The positive side of Dim1 grouped early stages characterized by higher starch content, greater firmness, and elevated mineral and structural components, whereas late stages were associated with increased soluble sugars, higher moisture content, enhanced enzymatic activity (PPO and POD), and pronounced color shifts. This opposition reflects the transition from a structural domain dominated by reserve compounds and mechanical integrity toward a solubilization domain characterized by tissue softening and oxidative processes. Such organization reinforces the interpretation of Dim1 as a parsimonious descriptor of ripening progression and highlights the potential of multivariate signatures to support objective maturity classification and future non-destructive monitoring strategies [5,35].

4.2. Coordination of Biochemical and Physical Changes During Ripening

Spearman's matrix (Figure 2) showed robust associations that allow the main axis to be interpreted in terms of coupled processes. The inverse relationship between AT and AR versus AL and °Brix ($\varrho \approx -0.99$) is consistent with the central phenomenon of the climacteric in bananas, the conversion of starchy reserves into soluble sugars. The directionality and magnitude of these changes are consistent with those reported for Cavendish cultivars under comparable conditions, suggesting sustained amylolytic behavior throughout the evaluated gradient [4,6].

Concomitantly, mechanical parameters showed a progressive loss of tissue structural performance, reflected in a decrease in maximum strength and modulus, along with changes in cohesiveness and adhesiveness (Table 8). This pattern is consistent with cell wall matrix rearrangement and changes in the pectic fraction that reduce stiffness and increase viscoplastic response, in line with evidence on cell wall modification pathways during banana ripening [36]. The negative association between Fmax and adhesiveness ($\varrho \approx -0.98$) suggests that softening is accompanied by greater deformability and stickiness, with direct implications for susceptibility to mechanical damage in postharvest handling.

The increase in PPO and POD during ripening and its correlation with stage progression ($\varrho \approx 0.98$) suggests intensification of the system's oxidative capacity in late stages. The relative increases in PPO (180.8%) and POD (219.9%) are relevant from the point of view of visual quality, given that both enzymes participate in phenolic substrate oxidation reactions and processes associated with browning, particularly when softened tissue increases its susceptibility to microlesions. The positive association with the a* parameter of the skin ($\varrho \approx 0.96$) is consistent with the intensification of reddish and brown tones typical of overripeness and with reports in climacteric fruits under post-harvest oxidative stress scenarios [37]. Consequently, the combination of PPO, POD, adhesiveness, and texture constitutes an informative block for anticipating the risk of visual deterioration, complementary to acceptance indicators such as °Brix.

Compared to the dominant variables of Dim1, vitamins mainly contributed to the secondary variation captured by Dim2. Vitamin C showed non-monotonic behavior, with a maximum in intermediate stages and a decrease towards late stages (Table 6), consistent with a dynamic balance between synthesis, recycling, and oxidative degradation during commercial maturity and overripeness [30]. Vitamins B1 and B6 remained within narrow ranges, suggesting relative stability

 doi:10.20944/preprints202602.2040.v1

and lower discriminating power compared to changes dominated by carbohydrates, texture, and oxidative activity.

4.3. Covariation of Color Attributes with the Physiological Axis of Ripening

The evolution of CIELAB parameters in the peel supports their usefulness as a non-destructive marker of ripening progress. The increase in L* and b*, together with the transition of a* from negative to positive values, is consistent with the degradation of chlorophylls and the accumulation of carotenoids during the climacteric, a pattern widely documented in bananas [15,38]. The alignment of these variables with the main axis of the PCA indicates that the visual component accompanies the overall physiological state of the fruit and captures a substantial part of the integrated variation.

However, the multivariate structure suggests that color should not be interpreted as a substitute for internal characterization. Its covariation with °Brix, texture, and PPO and POD activity indicates that color change is part of an integrated ripening syndrome but is not an independent predictor of critical attributes such as residual firmness or susceptibility to browning. This distinction is particularly relevant for computer vision monitoring strategies, where color classification may be adequate for operational segmentation by stages, while quantitative prediction of internal attributes requires calibration with mechanical and biochemical variables, or the use of multimodal approaches [15].

4.4. Implications for Postharvest Quality

The integration of the results allows the proposal of a functional segmentation scheme that complements visual classification and provides operational criteria for postharvest management. In early stages (T1–T3), fruits present higher mechanical integrity, predominance of starchy reserves, and lower oxidative activity, conditions compatible with greater tolerance to transport and storage and a reduced probability of visual deterioration induced by mechanical damage. In the transition stage (T4), accelerated carbohydrate metabolism and noticeable color changes occur while firmness remains moderate, defining a critical decision point for conservation strategies or controlled ripening induction.

Compared with previous studies focused mainly on physicochemical indicators or visual classification, the multivariate integration proposed here provides a more robust interpretation of maturity stages. By combining compositional, mechanical, chromatic, and enzymatic information within a single analytical framework, the present approach captures the coordinated nature of ripening more effectively than isolated indicators. This perspective aligns with recent trends in precision agriculture and data-driven postharvest management, where multidimensional datasets are increasingly used to support decision-making, optimize fruit allocation according to destination markets, and reduce postharvest losses through evidence-based classification strategies.

In intermediate stages oriented toward consumption (T5–T6), the increase in soluble solids combined with still manageable firmness and peak vitamin C levels describes an operational balance between sensory acceptability and remaining shelf life. However, the increase in PPO activity from these stages suggests the onset of higher susceptibility to oxidative processes. In advanced stages (T7–T9), the system converges toward greater carbohydrate solubilization, reduced rigidity, higher adhesiveness, and increased enzymatic activity, defining a profile suitable for immediate consumption or processing but with higher risk of rejection in fresh markets due to increased sensitivity to mechanical damage and visual deterioration [35].

5. Study Limitations

Sampling was restricted to a limited number of biological replicates per stage (n = 3) and to fruit obtained from a single acquisition scheme, which may limit the generalization of the findings to other batches, seasons, or agronomic conditions. In addition, stage classification was based on visual peel criteria, which may not fully reflect the internal physiological state of the fruit. Direct physiological

 doi:10.20944/preprints202602.2040.v1

indicators of the climacteric process, such as ethylene production or respiration rate, as well as molecular markers, were not included; therefore, mechanistic interpretations rely primarily on multivariate associations supported by previous literature. Furthermore, PCA and clustering analyses describe structural patterns and stage separation within the dataset but should not be interpreted as validated predictive models for operational classification beyond the evaluated sample.

Future studies should validate the proposed multivariate signatures under broader production conditions and larger sample sizes to assess their robustness and transferability for real-world postharvest monitoring applications.

6. Conclusions

Banana ripening exhibited a strongly coordinated multivariate organization dominated by a main physiological gradient, in which physicochemical, nutritional, mechanical, chromatic, and enzymatic variables co-varied systematically across maturity stages. The integration of these variables revealed a continuous transition from a structural state characterized by high starch content and mechanical integrity toward a solubilization state associated with sugar accumulation, tissue softening, and increased oxidative activity.

Beyond describing individual changes, the multivariate framework allowed the identification of functional ripening signatures that objectively differentiate maturity stages and provide a more comprehensive interpretation of the ripening process. This integrative perspective supports the use of multidimensional quality indicators as a basis for improving postharvest decision-making, fruit allocation strategies, and loss reduction along the supply chain.

Overall, the approach presented here bridges classical postharvest physiology with data-driven agriculture frameworks, establishing a conceptual foundation for the development of non-destructive monitoring systems and future intelligent tools for maturity assessment in banana production and commercialization systems.

Author Contributions: Conceptualization, F.G.-V., D.D.N.V., and J.D.V.-C.; methodology, F.G.-V. and R.I.B.Q.; software, M.J.Y.K.; validation, D.D.N.V. and F.G.-V.; formal analysis, F.G.-V. and R.I.B.Q.; investigation, F.G.-V., D.D.N.V., and R.I.B.Q.; resources, F.G.-V., D.D.N.V., and J.D.V.-C.; data curation, M.J.Y.K.; writing—original draft preparation, F.G.-V.; writing—review and editing, F.G.-V., D.D.N.V., M.J.Y.K., J.D.V.-C., and R.I.B.Q.; visualization, M.J.Y.K.; supervision, J.D.V.-C.; project administration, J.D.V.-C. and D.D.N.V.; funding acquisition, J.D.V.-C. All authors have read and agreed to the published version of the manuscript.

Funding: This research was funded by Universidad Estatal de Milagro (UNEMI).

Data Availability Statement: The raw data supporting the conclusions of this study will be made available by the authors upon reasonable request, without undue restrictions.

Acknowledgments: The authors gratefully acknowledge the support provided by the Universidad Estatal de Milagro (UNEMI) for the development of this research.

Conflicts of Interest: The authors declare no conflicts of interest. The research was conducted in the absence of any commercial or financial relationships that could be construed as a potential conflict of interest.

References

1. S. Martínez, A. Roman-Chipantiza, A. Boubertakh, and J. Carballo, “Banana Drying: A Review on Methods and Advances,” Food Rev. Int., vol. 40, no. 8, pp. 2188–2226, Nov. 2024, doi: 10.1080/87559129.2023.2262030.
2. G. E. Martínez-Solórzano and J. C. Rey-Brina, “Bananos (Musa AAA): Importancia, producción y comercio en tiempos de Covid-191,” Agron. Mesoam., vol. 32, no. 3, pp. 1034–1046, 2021, Accessed: Feb. 19, 2026. [Online]. Available: https://www.redalyc.org/journal/437/43768194023/html/
3. FAO, “Perspectivas a mediano plazo: perspectivas para la producción y el comercio mundial de bananos y frutas tropicales 2019-2028,” 2020.

 doi:10.20944/preprints202602.2040.v1

4. P.-H. Huang et al., "Changes in Nutrient Content and Physicochemical Properties of Cavendish Bananas var. Pei Chiao during Ripening," Horticulturae, vol. 10, no. 4, p. 384, Apr. 2024, doi: 10.3390/horticulturae10040384.
5. J. L. Moreno, T. Tran, B. Cantero-Tubilla, K. López-López, L. A. Becerra Lopez Lavalle, and D. Dufour, "Physicochemical and physiological changes during the ripening of Banana (Musaceae) fruit grown in Colombia," Int. J. Food Sci. Technol., vol. 56, no. 3, pp. 1171–1183, Mar. 2021, doi: 10.1111/ijfs.14851.
6. K. M. Phillips, R. C. McGinty, G. Couture, P. R. Pehrsson, K. McKillop, and N. K. Fukagawa, "Dietary fiber, starch, and sugars in bananas at different stages of ripeness in the retail market," PLOS ONE, vol. 16, no. 7, p. e0253366, Jul. 2021, doi: 10.1371/journal.pone.0253366.
7. A. A. R. Parijadi et al., "Metabolome Analysis of Banana (Musa acuminata) Treated With Chitosan Coating and Low Temperature Reveals Different Mechanisms Modulating Delayed Ripening," Front. Sustain. Food Syst., vol. 6, p. 835978, Mar. 2022, doi: 10.3389/fsufs.2022.835978.
8. J. Guo, J. Duan, J. Li, and Z. Yang, "Mechanized Technology Research and Equipment Application of Banana Post-Harvesting: A Review," Agronomy, vol. 10, no. 3, p. 374, Mar. 2020, doi: 10.3390/agronomy10030374.
9. M. Al-Dairi, P. B. Pathare, R. Al-Yahyai, H. Jayasuriya, and Z. Al-Attabi, "Postharvest quality, technologies, and strategies to reduce losses along the supply chain of banana: A review," Trends Food Sci. Technol., vol. 134, pp. 177–191, Apr. 2023, doi: 10.1016/j.tifs.2023.03.003.
10. S. D. T. Maduwanthi and R. A. U. J. Marapana, "Induced Ripening Agents and Their Effect on Fruit Quality of Banana," Int. J. Food Sci., vol. 2019, pp. 1–8, May 2019, doi: 10.1155/2019/2520179.
11. X. Zhang, L. Zhao, Q. Huang, B. Pang, Z. Zhou, and Y. Lu, "Synchronized fertilization based on crop nutrient uptake and fertilizer nutrient release characteristics increases nutrient use efficiency in banana," Sci. Rep., vol. 15, no. 1, p. 34449, Oct. 2025, doi: 10.1038/s41598-025-17602-0.
12. B. S. Everitt, S. Landau, M. Leese, and D. Stahl, Cluster Analysis, 1st ed. in Wiley Series in Probability and Statistics. Wiley, 2011. doi: 10.1002/9780470977811.
13. I. T. Jolliffe and J. Cadima, "Principal component analysis: a review and recent developments," Philos. Trans. R. Soc. Math. Phys. Eng. Sci., vol. 374, no. 2065, p. 20150202, Apr. 2016, doi: 10.1098/rsta.2015.0202.
14. K. Liakos, P. Busato, D. Moshou, S. Pearson, and D. Bochtis, "Machine Learning in Agriculture: A Review," Sensors, vol. 18, no. 8, p. 2674, Aug. 2018, doi: 10.3390/s18082674.
15. L. Ma et al., "Prediction of banana maturity based on the sweetness and color values of different segments during ripening," Curr. Res. Food Sci., vol. 5, pp. 1808–1817, 2022, doi: 10.1016/j.crfs.2022.08.024.
16. [S. Wolfert, L. Ge, C. Verdouw, and M.-J. Bogaardt, "Big Data in Smart Farming – A review," Agric. Syst., vol. 153, pp. 69–80, May 2017, doi: 10.1016/j.agsy.2017.01.023.
17. B. V. McCleary, T. S. Gibson, and D. C. Mugford, "Measurement of Total Starch in Cereal Products by Amyloglucosidase-α-Amylase Method: Collaborative Study," J. AOAC Int., vol. 80, no. 3, pp. 571–579, May 1997, doi: 10.1093/jaoac/80.3.571.
18. G. L. Miller, "Use of Dinitrosalicylic Acid Reagent for Determination of Reducing Sugar," Anal. Chem., vol. 31, no. 3, pp. 426–428, Mar. 1959, doi: 10.1021/ac60147a030.
19. J. L. Mason, "Flame Photometric Determination of Potassium in Unashed Plant Leaves.," Anal. Chem., vol. 35, no. 7, pp. 874–875, Jun. 1963, doi: 10.1021/ac60200a032.
20. B. A. Zarcinas, B. Cartwright, and L. R. Spouncer, "Nitric acid digestion and multi-element analysis of plant material by inductively coupled plasma spectrometry," Commun. Soil Sci. Plant Anal., vol. 18, no. 1, pp. 131–146, Jan. 1987, doi: 10.1080/00103628709367806.
21. R. Gertzen and M. Escobar, "Assays of Polyphenol Oxidase Activity in Walnut Leaf Tissue," BIO-Protoc., vol. 4, no. 16, 2014, doi: 10.21769/BioProtoc.1213.
22. D. R. Doerge, R. L. Divi, and M. I. Churchwell, "Identification of the Colored Guaiacol Oxidation Product Produced by Peroxidases," Anal. Biochem., vol. 250, no. 1, pp. 10–17, Jul. 1997, doi: 10.1006/abio.1997.2191.
23. Q. H. Ma, G. X. Wang, and L. S. Liang, "ESTABLISHMENT OF THE TEXTURAL DETECTING METHODS ON THE FRUIT OF CHINESE JUJUBE BY TEXTURE ANALYZER," Acta Hortic., no. 993, pp. 231–238, May 2013, doi: 10.17660/ActaHortic.2013.993.35.

 doi:10.20944/preprints202602.2040.v1

24. B. V. McCleary and D. A. Monaghan, “Measurement of Resistant Starch,” J. AOAC Int., vol. 85, no. 3, pp. 665–675, May 2002, doi: 10.1093/jaoac/85.3.665.
25. S. A. Jaywant, H. Singh, and K. M. Arif, “Sensors and Instruments for Brix Measurement: A Review,” Sensors, vol. 22, no. 6, p. 2290, Mar. 2022, doi: 10.3390/s22062290.
26. S. Marín-San Román, M. P. Diago, J. Fernández-Novales, R. Sánchez-Gómez, M. R. Salinas, and T. Garde-Cerdán, “NIR spectroscopy for predicting the aroma potential of intact tempranillo grape berries during ripening,” Eur. Food Res. Technol., vol. 251, no. 9, pp. 2731–2746, Sep. 2025, doi: 10.1007/s00217-025-04789-9.
27. International Organization for Standardization, Fruit and vegetable products — Determination of pH, ISO 1842, 1991. Accessed: Feb. 24, 2026. [Online]. Available: https://www.iso.org/es/contents/data/standard/00/65/6500.html
28. C. Tyl and G. D. Sadler, “pH and Titratable Acidity,” in Food Analysis, S. S. Nielsen, Ed., in Food Science Text Series. , Cham: Springer International Publishing, 2017, pp. 389–406. doi: 10.1007/978-3-319-45776-5_22.
29. Servicio Ecuatoriano de Normalización (INEN), Productos vegetales y de frutas – Determinación de la acidez titulable (IDT), NTE INEN-ISO 750, 2013. [Online]. Available: https://apps.normalizacion.gob.ec/descarga/index.php/buscar
30. E. Alós, J. Lado, M. Rodrigo, and L. Zacarías, “Citrus Fruit Ascorbic Acid Extraction and Quantification by HPLC,” BIO-Protoc., vol. 5, no. 5, 2015, doi: 10.21769/BioProtoc.1416.
31. G. W. Chase, W. O. Landen, A.-G. M. Soliman, and R. R. Eitenmiller, “Method Modification for Liquid Chromatographic Determination of Thiamine, Riboflavin, and Pyridoxine in Medical Foods,” J. AOAC Int., vol. 76, no. 6, pp. 1276–1280, Nov. 1993, doi: 10.1093/jaoac/76.6.1276.
32. M. J. Anderson, “Distance-Based Tests for Homogeneity of Multivariate Dispersions,” Biometrics, vol. 62, no. 1, pp. 245–253, Mar. 2006, doi: 10.1111/j.1541-0420.2005.00440.x.
33. S. Lê, J. Josse, and F. Husson, “FactoMineR : An R Package for Multivariate Analysis,” J. Stat. Softw., vol. 25, no. 1, 2008, doi: 10.18637/jss.v025.i01.
34. W. Shan et al., “Molecular characterization of banana NAC transcription factors and their interactions with ethylene signalling component EIL during fruit ripening,” J. Exp. Bot., vol. 63, no. 14, pp. 5171–5187, Sep. 2012, doi: 10.1093/jxb/ers178.
35. L. Wang et al., “Comparative analysis of physicochemical quality and metabolite profiles during fruit ripening in three banana cultivars using multivariate approaches,” Postharvest Biol. Technol., vol. 231, p. 113847, Jan. 2026, doi: 10.1016/j.postharvbio.2025.113847.
36. T. Ning et al., “Changes in Homogalacturonan Metabolism in Banana Peel during Fruit Development and Ripening,” Int. J. Mol. Sci., vol. 23, no. 1, p. 243, Dec. 2021, doi: 10.3390/ijms23010243.
37. F. Fang et al., “Impact of Allele-Specific Expression on Ripening and Quality Characteristics of ABB Banana Fruit,” Int. J. Mol. Sci., vol. 26, no. 9, p. 4090, Apr. 2025, doi: 10.3390/ijms26094090.
38. D. Laryea, S. Supapvanich, P. Pinsirodom, R. Suwapanich, S. Arsa, and J. Sirison, “Evaluating variety and ethephon effect on banana fruit quality at different ripening stages: A comparative and multivariate approach,” J. Agric. Food Res., vol. 19, p. 101569, Mar. 2025, doi: 10.1016/j.jafr.2024.101569.